Nonlinear vibrations of a composite beam in large displacements: Analytical, numerical, and experimental approaches

Nonlinear vibrations of a composite beam in large displacements: analytical, numerical and experimental approaches

Mattia Utzeri *†
Ph.D. Candidate
Department of Industrial Engineering and Mathematics
Università Politecnica delle Marche
Ancona, 60131
Italy
Email: m.utzeri@pm.univpm.it

Marco Sasso
Associate Professor
Department of Industrial Engineering and Mathematics
Università Politecnica delle Marche
Ancona, 60131
Italy
Email: m.sasso@univpm.it

Gianluca Chiappini
Assistant Professor
Department of Industrial Engineering and Mathematics
Università Politecnica delle Marche
Ancona, 60131
Italy
Email: g.chiappini@univpm.it

Stefano Lenci
Full Professor
Department of Civil and Building Engineering, and Architecture
Università Politecnica delle Marche
Ancona, 60131
Italy
Email: s.lenci@univpm.it

ABSTRACT

This paper investigates the nonlinear dynamic behavior of a cantilever beam made of composite material without and with lumped mass fixed along its length. The analysis compares the results coming from analytical and numerical modelling with experimental observations. The nonlinearities due to large vibration amplitude and to inertia effect are taken into account. An extended analytical approach has been developed, which is able to provide the approximate solution of the transverse displacement and the first nonlinear frequency with nonlinear terms up to fifth order. Then, an exact expression for the backbone curve is also proposed. In the experimental tests, a high speed imaging technique has been used to capture the vibrating behavior of a composite beam. Then, the nonlinearity of the acquired data is determined by the Fitting Time History technique. A Finite Element model has been implemented in order to validate the developed procedure. Finally, the results obtained by the analytical, experimental, and numerical methods are compared. It is found that the analytical formulation describes the real backbone curve of the beam, which is hardening. Accuracy of the analytical method decreases as the lumped mass increases.

INTRODUCTION

In the last few years, the use of composite materials (e.g. Carbon Fiber Reinforced Polymer, Glass Fiber Reinforced Polymer), foams, and polymers brought an increase of design of components in large deflection. Many engineering beam systems undergo large amplitude vibrations, such as aeroplane wings, fins, fishing-rods, paddles, which can be modelled as slender cantilever beams, with or without a lumped mass placed at given position along the length. Therefore, the use of linear vibration theory to analyze their dynamical behavior is insufficient. Only the nonlinear vibration theory allows establishing the correct dynamical behavior. Hence, many theoretical and experimental investigations of nonlinear vibrations of beams have appeared over the years [1, 2, 3, 4].

In general, the nonlinearity may be attributed to geometry (stiffness and inertia), and material

*Address all correspondence related to ASME style format and figures to this author.
†Address all correspondence related to ASME style format and figures to this author.

(constitutive equation and damping) [5]. Firstly, geometric nonlinearity are caused by large displacements and slopes. Consequently, it is not possible to use the small-angle assumption, which would reduce the nonlinear curvature to the simple linear form [6, 7, 8]. For a deeper discussion on the nonlinear curvature the reader is referred to [9, 10]. Nonlinear inertia effects may be caused by the presence of concentrated or distributed masses. Actually, for transverse vibrations of an initially straight beam there are transverse and axial inertial effects, both of them with linear and nonlinear contributions. In general, the transverse inertial effects cannot be neglected; on the contrary, the axial inertial effects are negligible in certain cases, e.g. for axially immovable boundary conditions [2, 11].

The nonlinear material effect may occur when the stresses are a nonlinear function of the strains [5]. This certainly occurs in plasticity, hysteretic materials, etc., but it may happen also in the elastic regime, as the one considered in this work. Besides, the nonlinearity may also appear as a consequence of peculiar boundary condition or contact between different components [12, 13, 14], or of more general discontinuities.

According to Hamdan [15, 16], the nonlinear stiffness induces nonlinear features of the hardening type, i.e., the vibration frequencies increase by increasing the amplitude of motion; this was also spotted by Wagner [17]. On the contrary, the inertial nonlinearity, which is related to the inextensibility condition and to the lumped mass, determines a softening behaviour of the so called backbone curve".

Nonlinear behavior of composite beam was widely investigated by experimental testing in literature. However, these studies mainly refer to nonlinearities due to material behavior, i.e. constitutive equation and damping. Many authors investigated on the nonlinear damping of composite beams, with special regard to the effect of the different type of reinforcement, such as fibers, graphene, fillers, and nanotubes [18, 19, 20]. On the other hand, the effects of geometric nonlinearity are less investigated. One of the few contributions was carried out by Lenci [21, 22], where the nonlinear frequency behavior of Glass Fiber Reinforced Polymer was investigated by means of Fitting Time History technique.

As regards the experimental equipment, today accelerometers are still the most used tech-

nique to measure the vibration response at known positions along the beams [18, 19, 20, 21, 22]; also laser technique has been used for the same purpose [23]. To the authors knowledge, on the contrary, modern imaging techniques have not been used yet with the aim of a combined analytical and experimental analysis of nonlinear vibrations.

The novelty of this study is to merge an extended analytical approach with experimental testing and numerical validation. The component considered for the analysis is a rectangular beam made of pre-preg Carbon Fiber Reinforced Polymer (CFRP) T700 TWILL, which is a fabric commonly used for the autoclave production of racing car components. The dynamic properties of these beams are of primary importance because they are used for high strength structural components which undergo large amplitude vibrations.

In the Analytical Method section of this paper, the effects of nonlinearity in a cantilever beam are addressed further elaborating and extending the analytical approach of the works [15, 17]. In particular, the nonlinear terms are expanded up to fifth order, and the rotational inertia of the lumped mass is included in the analytical equations of motion. Hence, enforcing stationarity of the lagrangian of the system yields to the unimodal equation, which can be solved by Multiple Scale Method [24]. Then, an exact expression for the backbone curve is proposed.In order to validate the analytical approach, experimental and numerical methods were also implemented.

The Experimental Method section shows the experimental test, where a high speed camera system was used to capture images of the beam subjected to large amplitude vibrations. Therefore, nonlinearity has been calculated using the entire profile of the beam and not just the individual measurements at the accelerometer or laser positions. The obtained results were post-processed by the Fitting Time History (FTH) technique, which is based on the least square approximation of general damped sinusoidal function with the measured free damped vibrations of the specimen. This technique allows to determine the main natural frequencies, the related modal damping coefficients, and damping and frequency nonlinearities [21, 22].

The Numerical Method section describes the numerical analysis of the cantilevered beam performed by the nonlinear transient solver of the commercial Finite Element software Ansys ©; the obtained oscillation amplitudes have been post-processed again with the FTH technique to

compute the numerical backbone curve.

Finally, the results of all methods, in terms of backbone curve and displacement oscillations of beams with and without lumped mass, are compared and discussed.

ANALYTICAL METHOD

The beam under consideration is shown in Fig.1. It is homogeneous, i.e. the cross-section, the density, and all other properties are constant along the beam axis. The lumped mass is fixed symmetrically with respect to the beam center line to maintain the symmetry with respect to the X reference line.

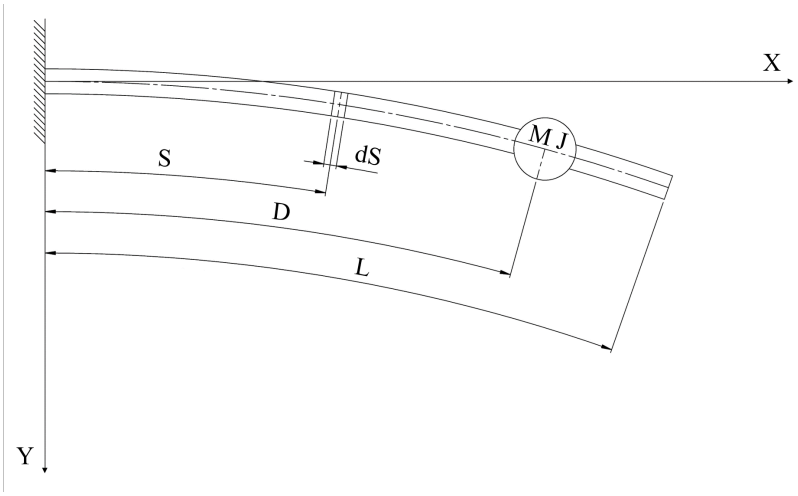

Fig. 1: Sketch of the beam system under study

The formulation takes into account large vibrations, the inextensibility of the beam, and the lumped mass inertial terms. As proposed by Hamdan [16], the equations of motion are determined starting from the definition of kinetic (E_k) and potential (E_p) energy of the beam:

$$E_k = \frac{mL^3}{2}\left[\int_0^1 (\dot{x}^2 + \dot{y}^2)d\zeta + \mu(\dot{x}^2 + \dot{y}^2)|_\eta + j\dot{\theta}^2|_\eta\right] \tag{1}$$

$$E_p = \frac{EI}{2L} \int_0^1 k(\zeta, t)^2 d\zeta \tag{2}$$

where dot means derivative with respect to time, $\zeta = \frac{S}{L}$ is the dimensionless distance from the left boundary, $x = \frac{X}{L}$ and $y = \frac{Y}{L}$. $X(\zeta, t)$ and $Y(\zeta, t)$ are the deformed position of the generic point $(\zeta, 0)$ in the reference straight configuration. $\eta = \frac{D}{L}$ is the given dimensionless position of the lumped mass. $\mu = \frac{M}{mL}$ and $j = \frac{J}{mL^3}$ are the inertia dimensionless parameters of the lumped mass. E is the elastic modulus and I is the area moment of inertia. The term $k(\zeta, t)$ is the curvature of the neutral axis of the beam, and is given by:

$$k = \theta' \tag{3}$$

where prime means derivative with respect to ζ, and θ is the rotation (equal to the beam slope, according to the Euler-Bernoulli beam):

$$\theta = \frac{dY}{dX} = \frac{dy}{dx} = \frac{y'}{x'} \tag{4}$$

In this work, as in [3], the axis of the beam is considered inextensible. This implies that:

$$x'^2 + y'^2 = 1 \tag{5}$$

namely,

$$x' = \sqrt{(1 - y'^2)} = 1 - \frac{y'^2}{2} - \frac{y'^4}{8} - \frac{y'^6}{16} + ... \tag{6}$$

where in the last expression a Taylor approximation is considered. By means of Eq.(6) we obtain, up to the due order,

$$\begin{aligned} \theta &= y' + \frac{y'^3}{2} + \frac{3y'^5}{8}, \\ \dot{\theta}^2 &= \dot{y}'^2(1 + 3y'^2 + 6y'^4) \end{aligned} \tag{7}$$

(use is made of the boundary condition $x(0) = 0$),

$$\begin{aligned} x &= \zeta - \int_0^\zeta \left(\frac{y'^2}{2} + \frac{y'^4}{8} + \frac{y'^6}{16} \right) d\chi, \\ \dot{x} &= -\int_0^\zeta \dot{y}' \left(y' + \frac{y'^3}{2} + \frac{3y'^5}{8} \right) d\chi \end{aligned} \tag{8}$$

and

$$k = y'' \left(1 + \frac{3y'^2}{2} + \frac{15y'^4}{8} \right) \tag{9}$$

Note that the higher order terms are positive, meaning that the curvature increases (with respect to the linear case) for increasing amplitudes. This explains the hardening behavior due to the geometric stiffness nonlinearity.

The expression of the kinetic energy of the system then becomes:

$$\begin{aligned} E_k = \frac{mL^3}{2} \Bigg\{ & \int_0^1 \left[\dot{y}^2 + \left(\int_0^\zeta \dot{y}' \left(y' + \frac{y'^3}{2} + \frac{3y'^5}{8} \right) d\chi \right)^2 \right] d\zeta \\ & + \mu \left[\dot{y}^2 + \left(\int_0^\zeta \dot{y}' \left(y' + \frac{y'^3}{2} + \frac{3y'^5}{8} \right) d\chi \right)^2 \right]_\eta \\ & + j \left[\dot{y}'^2(1 + 3y'^2 + 6y'^4) \right]_\eta \Bigg\} \end{aligned} \tag{10}$$

Likewise, the potential energy becomes:

$$E_p = \frac{EI}{2L}\int_0^1 y''^2\left(1+\frac{3y'^2}{2}+\frac{15y'^4}{8}\right)^2 d\zeta \tag{11}$$

We consider a monomodal response, namely we assume that:

$$y(\zeta,t) = u(t)\Phi(\zeta) \tag{12}$$

where $\Phi(\zeta)$ is a given function and $u(t)$ is the unknown.

For the same purpose, the beam motion could be formulated by a more complex spatial function along with damping as done in [25, 26], where the multiple-timescales perturbation method was applied to construct approximations of the problem solution in place of the monomodal approach.

After some computations we get

$$\begin{aligned} E_k &= \frac{mL^3}{2}\dot{u}^2(\alpha_1+\alpha_2u^2+\alpha_3u^4),\\ E_p &= \frac{EI}{2L}u^2(\alpha_4+\alpha_5u^2+\alpha_6u^4) \end{aligned} \tag{13}$$

where

$$
\begin{aligned}
\alpha_1 &= \int_0^1 \Phi^2(\zeta)d\zeta + \mu\Phi(\eta)^2 + j\Phi'(\eta)^2, \\
\alpha_2 &= \int_0^1 \left(\int_0^\zeta \Phi'^2(\chi)d\chi\right)^2 d\zeta + \mu\left(\int_0^\eta \Phi'^2(\chi)d\chi\right)^2 + 3j\Phi'(\eta)^4, \\
\alpha_3 &= \int_0^1 \left(\int_0^\zeta \Phi'^2(\chi)d\chi\right)\left(\int_0^\zeta \Phi'^4(\chi)d\chi\right) d\zeta, \\
&\quad + \mu\left(\int_0^\eta \Phi'^2(\chi)d\chi\right)\left(\int_0^\eta \Phi'^4(\chi)d\chi\right) + 6j\Phi'(\eta)^6, \\
\alpha_4 &= \int_0^1 \Phi''^2(\zeta)d\zeta, \\
\alpha_5 &= 3\int_0^1 \Phi''^2(\zeta)\Phi'^2(\zeta)d\zeta, \\
\alpha_6 &= 6\int_0^1 \Phi''^2(\zeta)\Phi'^4(\zeta)d\zeta
\end{aligned}
\tag{14}
$$

In the following Φ is assumed to be a linear mode of the beam without lumped mass, i.e.:

$$
\begin{aligned}
\Phi(\zeta) &= c_1\{[\sin(p\zeta) - \sinh(p\zeta)] - c_2[\cos(p\zeta) - \cosh(p\zeta)]\}, \\
p^4 &= \frac{\omega_{n0}^2}{\beta^2}, \\
\beta &= \sqrt{\frac{EI}{mL^4}}, \\
c_2 &= \frac{\sin(p) + \sinh(p)}{\cos(p) + \cosh(p)}, \\
c_1 &= \frac{1}{2}\frac{\cos(p)\cosh(p)}{\sin(p)\cosh(p) - \cos(p)\sinh(p)}
\end{aligned}
\tag{15}
$$

Note that the previous choice of c_1 guarantees that $\Phi(1) = 1$, which in turn implies that $u(t)$ is the transversal position of the tip point of the beam. ω_{n0} is the natural (linear) frequency of the beam without lumped mass. It dimensionless version p can be computed by the frequency equation

$$
\cosh(p)\cosh(p) + 1 = 0 \tag{16}
$$

The first solution of Eq.(16) is $p_1 = 1.875104$, that for $\eta = 0.975$ provides:

$$\begin{aligned}
\alpha_1 &= 0.25 + 0.9323593413\,\mu + 1.8946794834\,j,\\
\alpha_2 &= 0.2872982813 + 1.2422795395\,\mu + 10.7694310340\,j,\\
\alpha_3 &= 0.4004741163 + 1.9061922898\,\mu + 40.8092400552\,j,\\
\alpha_4 &= 3.0905908421,\\
\alpha_5 &= 3.7913121985,\\
\alpha_6 &= 6.6926625781
\end{aligned} \tag{17}$$

The lagrangian of the system is defined as $\ell = E_k - E_p$. Inserting the Eq.(13) in ℓ, and enforcing stationariety, the unimodal equation [15, 27] is achieved:

$$\ddot{u}(\alpha_1 + \alpha_2 u^2 + \alpha_3 u^4) + \dot{u}^2(\alpha_2 u + 2\alpha_3 u^3) + \beta^2(\alpha_4 u + 2\alpha_5 u^3 + 3\alpha_6 u^5) = 0 \tag{18}$$

where the nonlinear inertial terms are clearly visible.

In the present study $\Phi(\zeta)$ is the true eigenfunction of the linear problem neglecting the attached lumped mass. It is used for reasons of simplicity and computational effort but at the expense of reduced accuracy, especially for big lumped masses; as will be illustrated in the results section, the lack of accuracy is small for small attached mass M. The true eigenfunctions, which take complicated forms, can be obtained by solving the linear problem. Liu and Huang obtained the solution by using the Laplace transform method [28]; however they show only the first true eigenfunction with attached mass, which is close to the case without the mass.

Furthermore, Hamdan highlighted the analytical differences between these two cases [29]; he confirmed the accuracy of the results using the first true eigenfunction without attached mass with mass ratios μ lower than 3 [16].

The Eq.(18) is solved by the Multiple Scale Method [24], and the approximate solution is given

by

$$u(t) = A\sin(\omega_{nl}t + \phi) + \frac{1}{16}\left(\frac{\alpha_5}{\alpha_4} - \frac{\alpha_2}{\alpha_1}\right)A^3\sin[3(\omega_{nl}t + \phi)] + ... \tag{19}$$

The ω_{nl} is the nonlinear frequency, and can be written in the form

$$\omega_{nl} = \omega_{n0} + \omega_{n2}A^2 + \omega_{n4}A^4 + ... \tag{20}$$

where:

$$\begin{aligned}
\omega_{n0} &= \beta\sqrt{\frac{\alpha_4}{\alpha_1}}, \\
\omega_{n2} &= \frac{\omega_{n0}}{4}\left(3\frac{\alpha_5}{\alpha_4} - \frac{\alpha_2}{\alpha_1}\right), \\
\omega_{n4} &= \frac{\omega_{n0}}{64}\left(-15\frac{\alpha_5^2}{\alpha_4^2} - 18\frac{\alpha_2\,\alpha_5}{\alpha_1\,\alpha_4} + 9\frac{\alpha_2^2}{\alpha_1^2} + 60\frac{\alpha_6}{\alpha_4} - 12\frac{\alpha_3}{\alpha_1}\right)
\end{aligned} \tag{21}$$

Eq.(20) is the analytical expression of the backbone curve, approximated up to the fifth order.

For the case of Eq.(17), and for $\mu = j = 0$ (i.e. no lumped mass), we have

$$\begin{aligned}
\omega_{10} &= 3.516015\,\frac{\sqrt{EI}}{L^2\sqrt{m}}, \\
\omega_{12} &= \omega_{10}\,0.632747, \\
\omega_{14} &= \omega_{10}\,1.166320
\end{aligned} \tag{22}$$

The fact that $\omega_{12} > 0$ prove that the beam has an hardening behavior, that increases its hardening nature for increasing amplitudes, since also $\omega_{14} > 0$.

The physical tranvsersal position of the beam, which is needed for comparison with numerical

and experimental results, is given by

$$Y(\zeta,t) = L\,\Phi(\zeta)\,u(t) \tag{23}$$

where $u(t)$ is given by Eq.(19). Considering only the first term in Eq.(19), we have that in each position ζ the maximum displacement in time is given by

$$Y_{\max}(\zeta) = L\,\Phi(\zeta)\,A \tag{24}$$

so that Eq.(20) becomes

$$\omega_{nl} = \omega_{n0} + \omega_{n2}\left[\frac{Y_{\max}(\zeta)}{L\,\Phi(\zeta)}\right]^2 + \omega_{n4}\left[\frac{Y_{\max}(\zeta)}{L\,\Phi(\zeta)}\right]^4 + ... \tag{25}$$

Although it will not be used here, since Eq.(20) is more than sufficient for the scope of the present paper, it could be interesting to note that, exploiting the conservation of energy, it is possible to obtain the following *exact* expression for the backbone curve:

$$\omega_{nl}(A) = \frac{\pi}{2}\frac{1}{\int_0^A \frac{du}{\sqrt{\frac{\alpha_4(A^2-u^2)+\alpha_5(A^4-u^4)+\alpha_6(A^6-u^6)}{\alpha_1+\alpha_2u^2+\alpha_3u^4}}}} \tag{26}$$

EXPERIMENTAL METHOD

The pre-preg CFRP is the most used composite materials for the production of high strength structural components. Accordingly, the specimen was chosen in CFRP T700 TWILL, which is a fabric commonly used for the production in autoclave of different racing car components as monocoque, bodyworks, suspension components, wings, etc.

The beam linear density m is 0.0681 $\frac{Kg}{m}$. The flexural Young's modulus E was determined experimentally through the standard test method for flexural properties of polymer matrix composite materials (ASTM D7264/D7264M); its value was found to be 44951 $\frac{N}{mm^2}$. The geometric properties of the specimen are:

1. The beam cross-section is rectangular, where the base is 25.05 mm and the height is 1.85 mm. So, the moment of inertia I is 13.2173 mm^4;
2. The length of the beam is to 205 mm;
3. The fibers are oriented at 0° along its length.

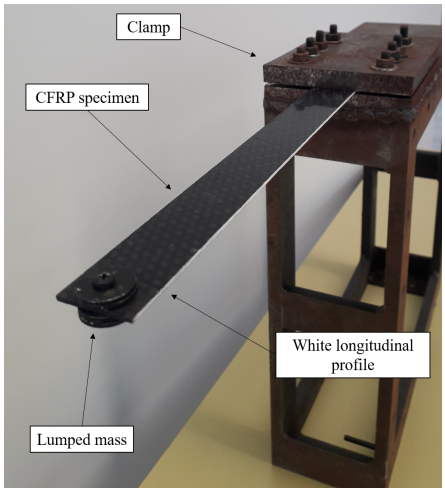

Fig. 2: The CFRP specimen

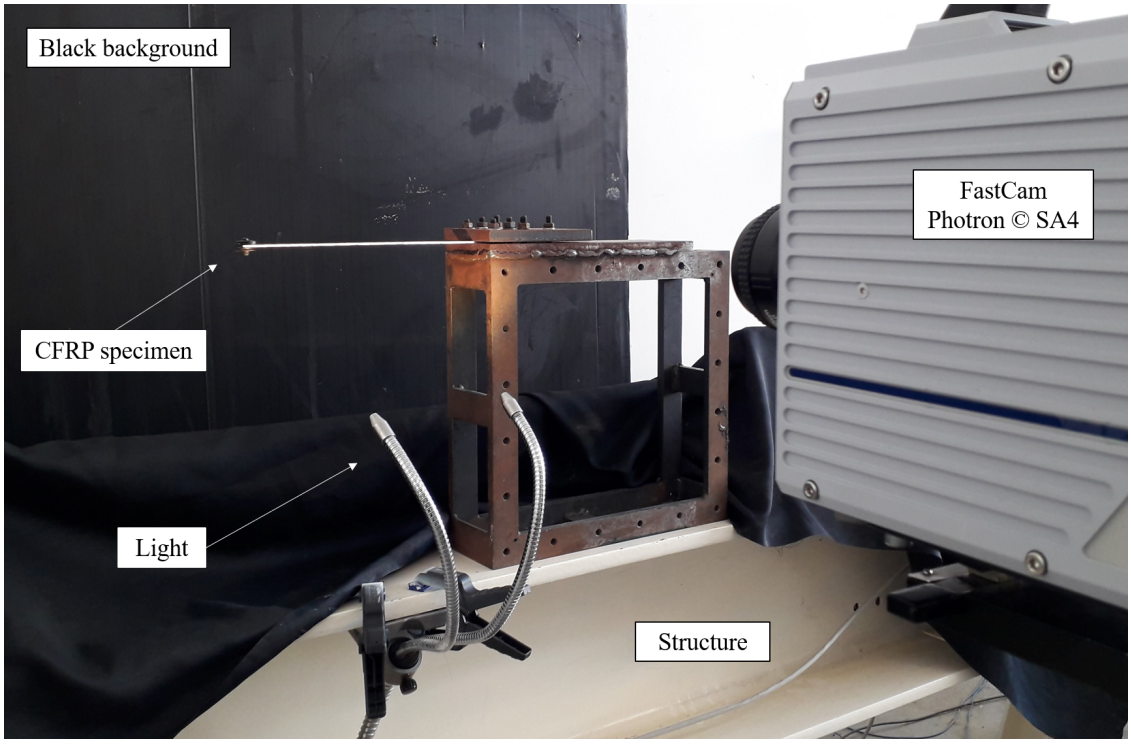

Fig. 3: Setup of the experimental test

The specimen is bonded to a highly rigid structure, as shown in Fig.3. The lumped mass is fixed symmetrically trough a bolt on the beam, as shown in Fig.2, in order to prevent an asymmetric behavior and to avoid any possible sliding of the mass during the oscillation. The bolt used to fix the added mass was included in the calculation, in terms of both translational and rotational inertia. Masses were measured by means of high precision balance. The inertia matrix was calculated by a detailed CAD model in Solidworks©.

In the experimental test, the specimen is subjected to an impulse at its free end, and the oscillation amplitude is measured along time. During beam oscillations, gray level images were acquired for 2 seconds by a high speed camera (model FastCam Photron ©SA4) at 10,000 frame per second.

The measurement of the displacement of each point is made by arranging the camera transversely to the specimen. In this way, it was possible to visualize the movement of the longitudinal section of the beam. The optics and lighting setup were arranged in such a way that the profile of

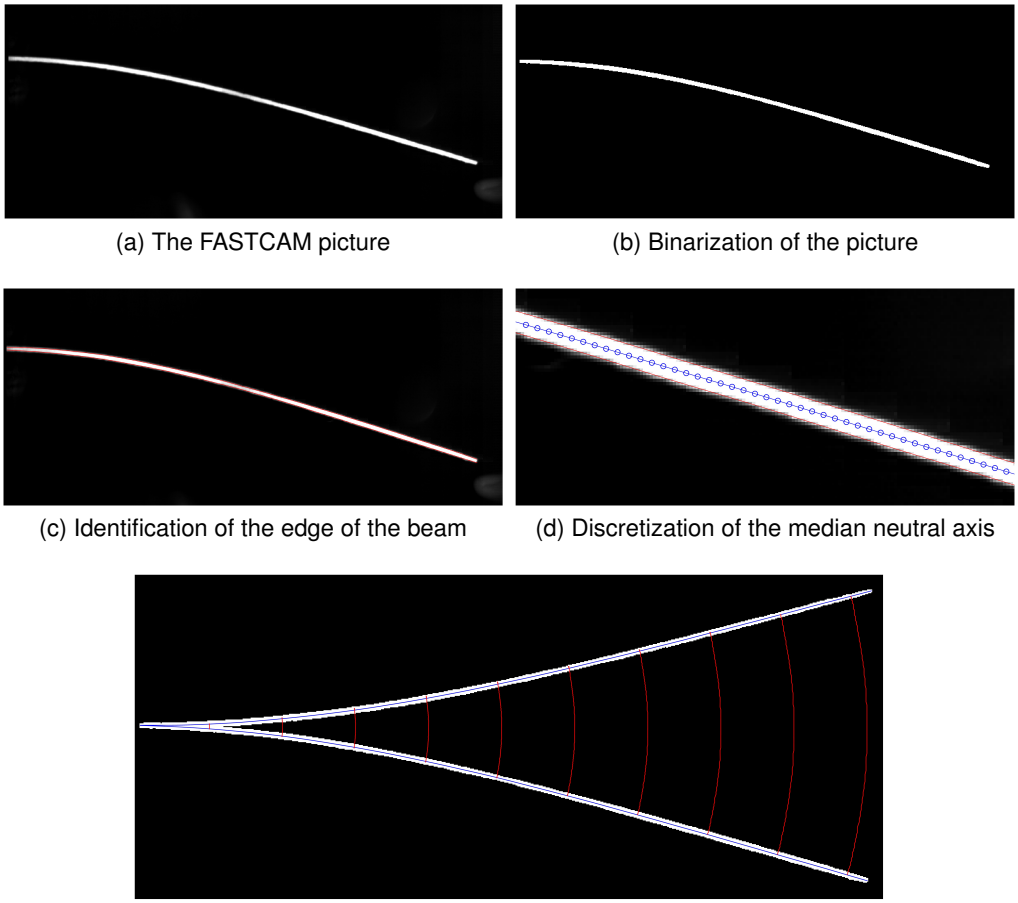

(a) The FASTCAM picture

(b) Binarization of the picture

(c) Identification of the edge of the beam

(d) Discretization of the median neutral axis

(e) Position of any point of the beam during the test. The trajectory of the point is in red

Fig. 4: Image processing

the longitudinal section appears as a white line on a black background. By means of the Matlab Image Processing toolbox, each picture has been processed in order to obtain the profile of beam longitudinal section, as shown in Fig.4.

In detail, the Fig.4a shows a picture of longitudinal section of the beam during an oscillation, and the Fig.4b shows its binarization in Matlab (1 white and 0 black). In this way, the upper and the lower edge of the longitudinal profile were identified (red lines in Fig.4c), from which the median neutral axis was obtained (the blue line between the red lines in Fig.4d). The neutral axis was discretized through the line integral so each point (blue circles in Fig.4d) corresponds to the same physical point in all acquired images. Fig.4e shows the trajectory (red lines) of ten points during

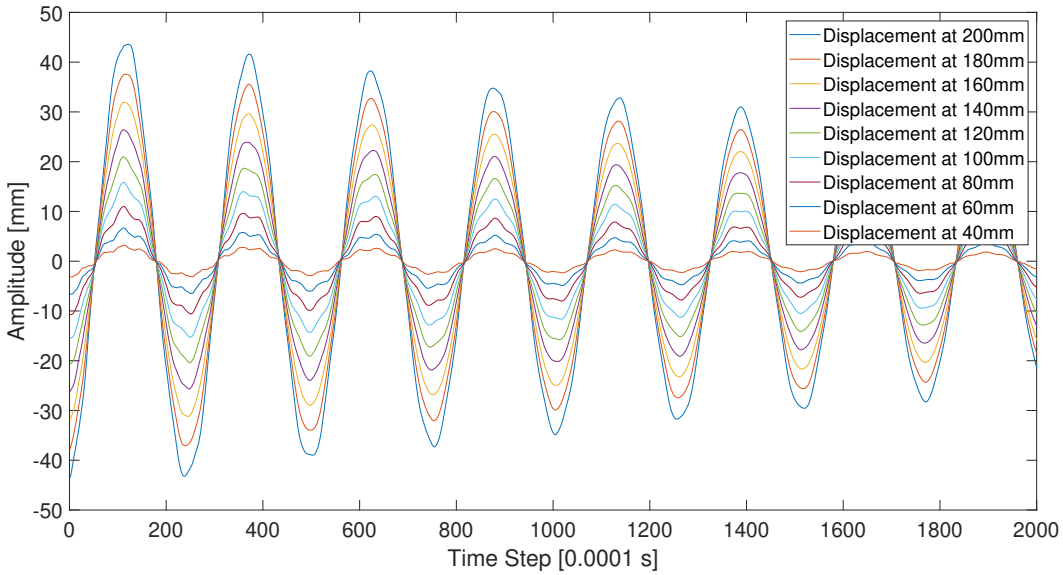

Fig. 5: The displacement of some point of the beam

half oscillation of the beam between the lower and upper position. Figure 5 shows the output of the image analysis, i.e. the displacement as a function of time of the ten points shown in Fig.4e, after an impulsive excitation.

Nonlinearities identification

Following [22, 21], the results were post-processed by the Fitting Time History (FTH) technique, which is based on the least square approximation of the measured free damped vibrations. FTH is a well-known technique for the vibration analysis of any kind of structure and material. This identification technique belongs to the family of time correction method, often used for the investigation of the dynamic response of a bridge under normal vehicular loads as well as under exceptional earthquake loads [30, 31]. FTH starts from the observation that, in free vibrations, the single $i-th$ mode system response is defined by single free damped vibration, as in multi-modal approach. So, FTH technique allows to reveal how both natural frequencies and modal damping coefficients depend nonlinearly on the excitation amplitude for each mode. According to Eq.(19), and retaining only the term proportional to A, the amplitude q_i of the i-th mode during the free

oscillations is given by

$$q_i(t) = A_i(t) \sin(\omega_{iD} t + \phi_i) \tag{27}$$

where $A_i(t) = B_i e^{-\xi_i \omega_i t}$ represents the oscillation amplitude, which is assumed to vary in time because of the damping. $\omega_{iD} = \omega_i \sqrt{(1-\xi_i)}$ is the damped frequency, ω_i is the natural frequency, ξ_i is the damping coefficient and B_i and ϕ_i are the starting amplitude and the phase delay, respectively, that depend on the initial conditions. The linear frequency is initially, and temptatively, obtained by the Fast Fourier Transform (FFT). The previous section showed that the nonlinear frequency is a function of the amplitude. Thus, according to Eq.(20), we assume:

$$\omega_i(t) = \omega_{i0} + \omega_{i2} A_i^2(t) + \omega_{i4} A_i^4(t) \tag{28}$$

where ω_{i0} is the linear (natural) frequency and ω_{ij} are the nonlinear correction terms of j-th order for the i-th mode. Consistently with the above explained approach, the nonlinear damping has been assumed as:

$$\xi_i(t) = \xi_{i0} + \xi_{i1} A_i(t) + \xi_{i2} A_i^2(t) \tag{29}$$

FTH optimization needs a cost or error function to be minimized. Therefore, the normal root means square deviation (NRMSD) between analytical function and experimental measures is used:

$$NRMSD(\xi_{ij}, \omega_{ij}, \phi_i, B_i) = \frac{\sqrt{\frac{\sum_{k=1}^{N} (q_k - \widehat{y_k})^2}{N}}}{max\,|\widehat{y}|} \tag{30}$$

where N is the number of acquired samples, $\widehat{y_k}$ is the k-th experimental observation, q_k is the value of the analytical function at the same time.

Introducing the nonlinearity into Eq.(27) and proceeding with the minimization algorithm, the NRMSD provides the optimal estimation of the mechanical properties of the system, i.e. the linear terms ω_{i0} and ξ_{i0}, and the nonlinear terms ω_{i2}, ω_{i4}, ξ_{i1} and ξ_{i2}. To improve the approximation of the experimental signal, and to detect also higher order modal parameters, more terms are added:

$$q_i(t) = \sum_{i=1}^{P} A_i(t) \sin\left(\omega_i D t + \phi\right) \tag{31}$$

where P is the number of modes considered.

The minimization algorithm was created in-house with Matlab ©. Finally, the nonlinear damping an frequency coefficients were progressively introduced into the Matlab optimization algorithm: first, only linear terms where considered, then a second term was added, and so on. The performance of the optimization algorithm was observed to improve increasingly.

NUMERICAL METHOD

The FEM analysis was carried out by the ANSYS APDL ©software. The first step of the FEM analysis was to define the material and the geometrical characteristic. The material has been defined as a linear orthotropic material, that is described only by Young's modula and Poisson's coefficients $E_{11}, E_{22}, \nu_{12}, \nu_{21}$.

The beam has been meshed with 1,000 beam elements. Typically, a discretized model is more rigid than the real case so that the real frequency is overestimated by FEM; therefore increasing the number of elements can reduce this misleading phenomenon. Before the nonlinear analysis, the modal analysis was carried out to validate the model at least in the linear regime. Then, the free oscillation was simulated applying a 10 N impulsive force, in a direction orthogonal to the length, at the free end of the beam, and the nonlinear transient solver has been used to compute the time history of the entire beam deflection. A very small time step, i.e. 0.00001 s, has been

used in the FEM simulation, and the displacement results were recorded at intervals of 0.0001 s, replicating the same sampling rate adopted in the real experiments.

The FEM output results have been processed with the same identification approach proposed in the case of the experimental test.

It is worth noting that Ansys APDL allows to assign the damping as Rayleigh damping, which consists of a linear combination of the stiffness and mass matrices. In the experimental tests, the approximation of the free oscillations solution with the first and the second mode allows to obtain the coefficients of α and β at the base of the damping model. The damping matrix is defined as $\boldsymbol{C} = \alpha\boldsymbol{M} + \beta\boldsymbol{K}$, and α and β are determined by:

$$\begin{cases} 2\omega_{n1}\xi_1 = \alpha + \beta\omega_{n1}^2, \\ 2\omega_{n2}\xi_2 = \alpha + \beta\omega_{n2}^2 \end{cases} \tag{32}$$

$$\beta = \frac{2(\xi_1\omega_{n1} - \xi_2\omega_{n2})}{(\omega_{n1}^2 - \omega_{n2}^2)} \tag{33}$$

$$\alpha = \omega_{n1}(2\xi_1 - \beta\omega_{n1}) \tag{34}$$

RESULTS AND DISCUSSION

The results obtained by the analytical, experimental and numerical methods applied to the cantilever beam without lumped mass are first discussed individually. Then, a comparison among the three methos is presented; the effect of a lumped mass at 97.5% of the beam length from the fixed support is also considered. The backbone curves behavior and the consistency of the

models are assessed.

Analytical results

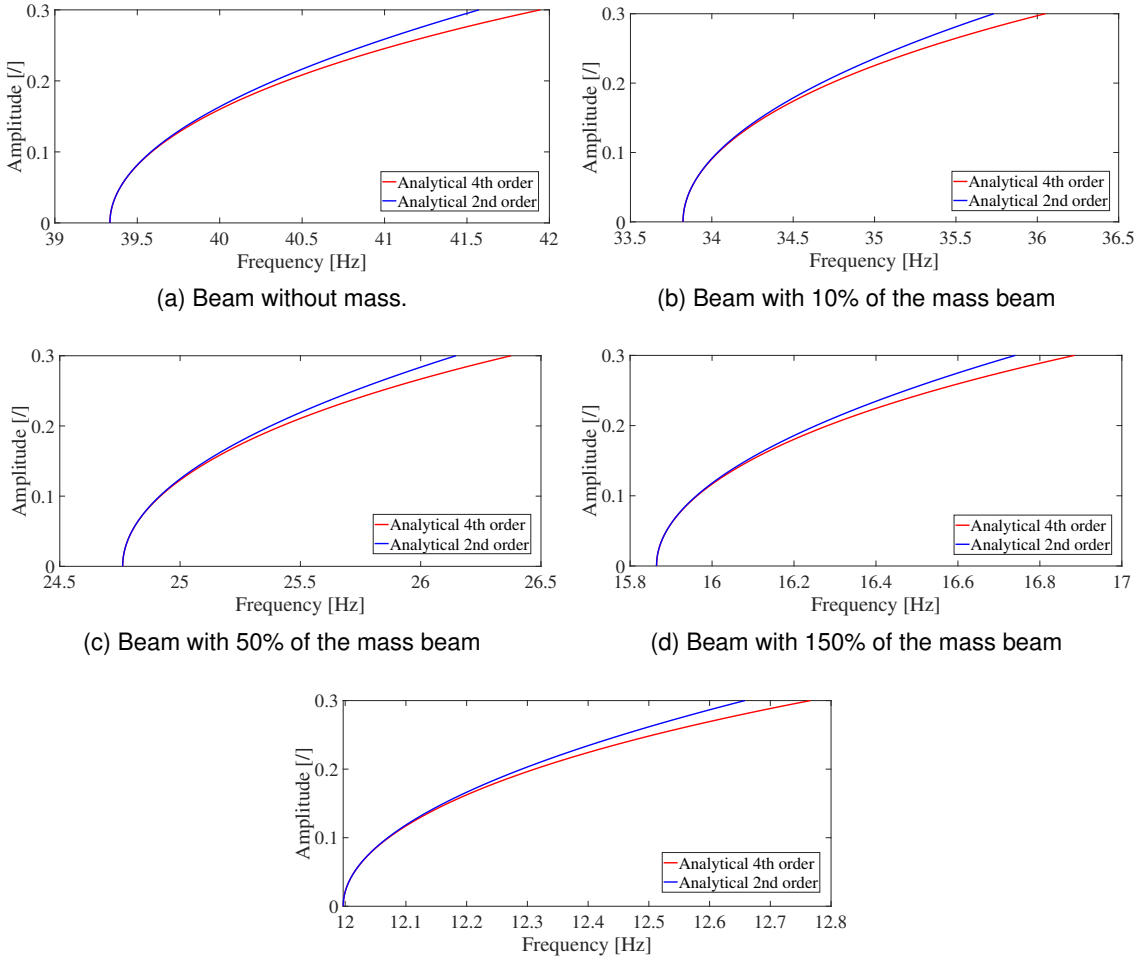

(a) Beam without mass.

(b) Beam with 10% of the mass beam

(c) Beam with 50% of the mass beam

(d) Beam with 150% of the mass beam

(e) Beam with 300% of the mass beam

Fig. 6: Comparison of backbone curves determined by analytical method

Figure 6 shows the backbone curves associated with the first frequency, computed by the analytical formulation, by considering the terms in Eq.(20). The related parameters are reported in Tab. 1.

The formulation predicts a hardening backbone curve, where the fourth order term is relevant only for large amplitudes. Indeed, the curves are basically superimposed for low amplitudes. The

$\omega_{1j}[\frac{rad}{s}]$	No mass (a)	10% (b)	50% (c)	150% (d)	300% (e)
ω_{10}	247.1430	214.5621	159.5827	103.3850	78.4830
ω_{12}	156.3003	133.2327	96.6669	61.2898	46.2269
ω_{14}	287.9527	245.4494	178.1913	112.5987	84.1152

Table 1: First analytical nonlinear frequency terms

curves in Fig.6 demonstrates that inertial nonlinearities in each backbone curve are slightly less important than geometrical ones, since the behavior of the curved backbone is still hardening. However, the inertial nonlinearity cannot be neglected in the model. Indeed, the Tab. 1 shows the effect of inertial terms: the larger the lumped mass M the lower the hardening behavior (which is measured by ω_{12}). The curves do not change significantly for large amplitudes but reduce the nonlinear terms. As a consequence, it can be argued that the backbone curve can switch from hardening to softening type with a huge mass.

Experimental results

The FTH technique has been applied to the displacement signals measured in the experiment described in Section .

The coefficients of the FTH fittings, which synthesize the experimental results, are reported in Tab. 2, together with the achieved NRMSD values. It can be noted that, as expected, the NRMSD values reduces as the modelling is enhanced from linear unimodal to nonlinear multimodal. The ϕ_2, B_2, ϕ_1, B_1 terms do not have a role in the system characterization; they appear only in the minimization algorithm, and are reported for completeness of information. Fig.7 shows the results in terms of free oscillations amplitude vs time at the free end of the beam; the values measured by image analysis are compared with the linear (Fig.7a), and nonlinear multimodal (Fig.7b) FTH fittings. The matching between experimental and FTH reconstructed curves is very good, especially for the nonlinear multimodal identification. For the sake of clarity, an enlargement of the curves of previous Fig.7b are reported in Fig.8a; it can be seen that the correspondence is optimal even after 2-3 seconds of free oscillations. The enlargement presented in Fig.8b refers to a point located

	Unimodal linear	Unimodal first order nonlinearities	Unimodal second order nonlinearities	Multimodal
	Fig.7 (a)	-	-	Fig.7 (b)
NRMSD	4.14%	2.64%	1.07%	0.76%
ω_{10}	247.1473	247.1488	247.1538	247.1528
ω_{12}	0	102.1269	134.2156	162.2321
ω_{14}	0	0	248.5231	264.6589
ξ_{10}	0.0091	0.0088	0.0063	0.0076
ξ_{11}	0	0.1910	0.3431	0.1793
ξ_{12}	0	0	-6.0519	-4.0536
B_1	0.2426	0.2433	0.2451	0.2475
ϕ_1	1.3219	1.3184	1.3170	1.2907
ω_{20}	0	0	0	1549.5
ξ_{20}	0	0	0	0.0041
B_2	0	0	0	-0.0012
ϕ_2	0	0	0	3.0167

Table 2: FTH fitting coefficients for the signal at 97.5% of the beam length

39% of the beam length away from the fixed support. In the graph in Fig.8 it can be seen that in the signal at 97.5% of the beam length the presence of the superharmonic (multimodal) terms is much less evident than in the case in which the displacement is sampled at 39% of the beam length. Indeed, the amplitude associated to the first mode is larger than the other modes, consequently, the temporal evolution of the displacement of this point is a nearly perfect damped sine curve. Instead, the signal at 39% of the beam length is more influenced by other natural shape modes, since their amplitudes are comparable with that of the first mode. The fitting is excellent even in this case, where the oscillations are more disturbed.

Fig.9 shows the trend of the backbone curves associated with the first frequency, computed by FTH methods on experimental signals and compared with those obtained by the analytical model.

The experimentally reconstructed backbone curve has an excellent agreement with those obtained with analytical formulation, confirming the reliability of the model and, in turn, relevance of geometrical and inertial nonlinearities. Moreover, as expected, multimodal identification increases

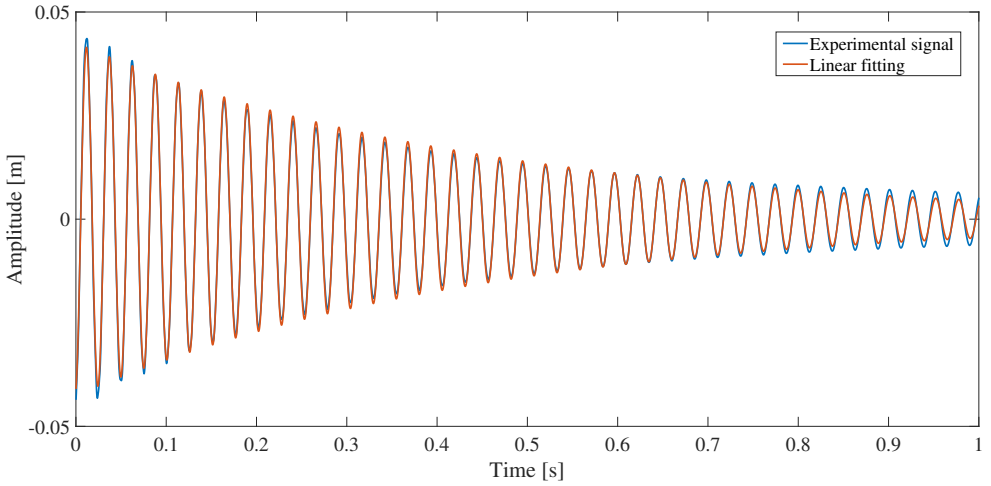

(a)

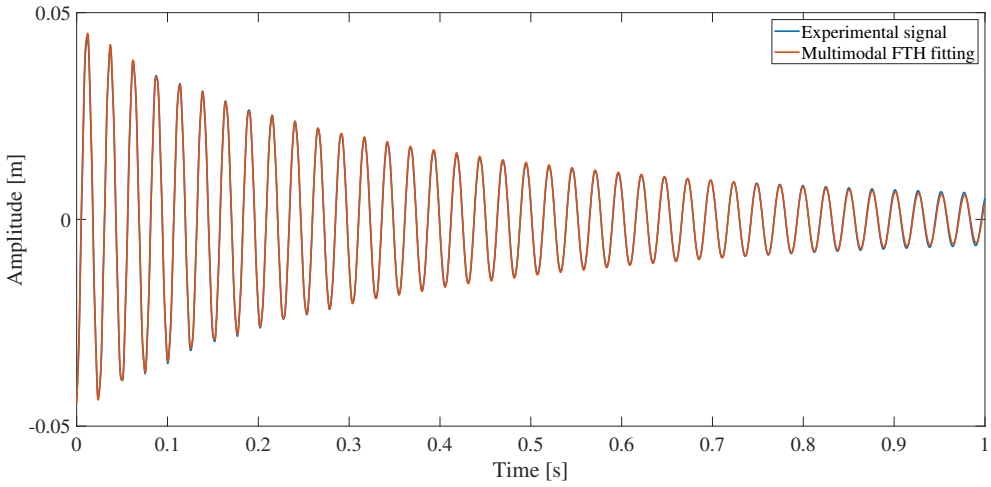

(b)

Fig. 7: Comparison of experimental signals and FTH fittings.(a) Linear Fitting. (b) First and second nonlinear frequency and nonlinear damping fitting

the performance of the FTH. Indeed, including the second mode with its relative nonlinearities, the backbone curve approaches the one obtained analytically: this is numerically confirmed by the fact that ω_{12} passes from 102.12 to 162.23 (see Tab. 2), which is closer to the theoretical value 156.30 (see Tab. 1).

Finally, Fig.10a shows a direct comparison between the backbone curves, reconstructed by FTH. The points at 39% and 97.5% of the beam length are labelled as A_1 and A_2, respectively, for the vibration frequency of 39.35 Hz. The same points at 39% and 97.5% of the beam length

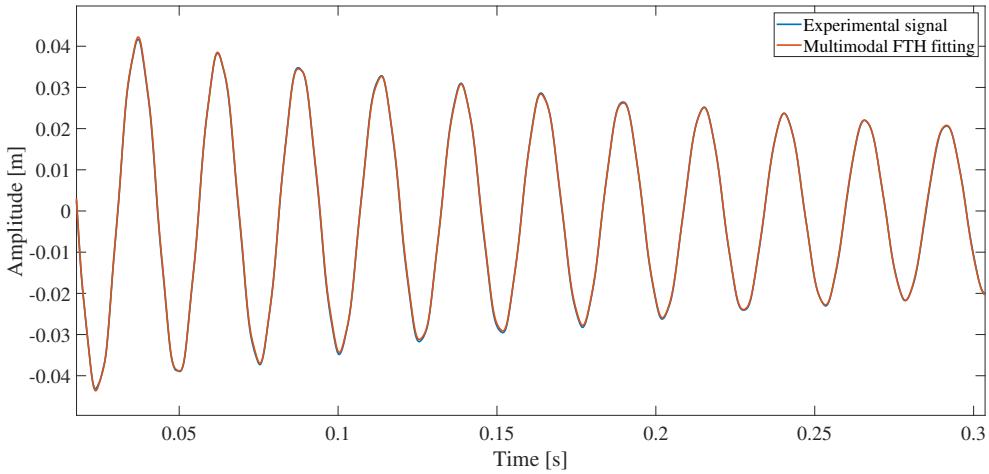

(a) Signal at 97.5% of the beam length

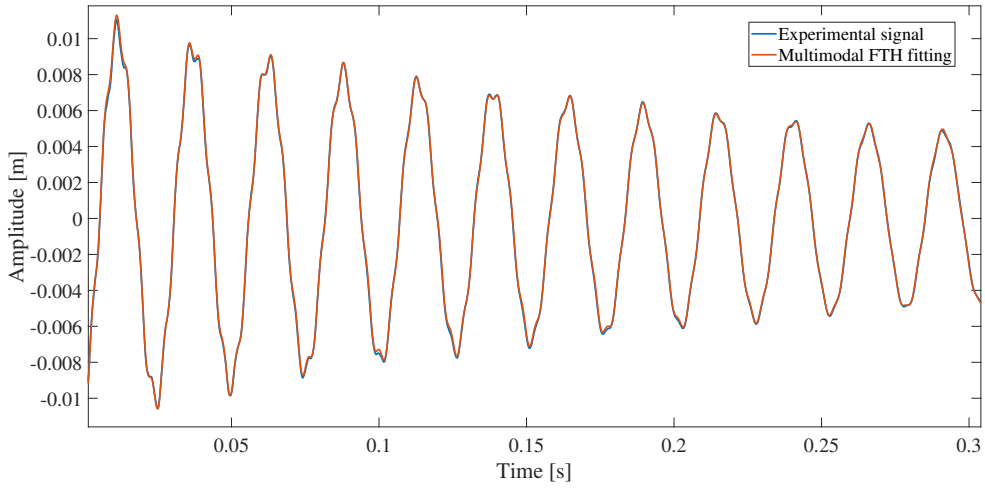

(b) Signal at 39% of the beam length

Fig. 8: Comparison of experimental signal with signal obtained by FTH identification

are labelled as A_5 and A_6 for the frequency 39.375 Hz. The amplitudes at 39% and 97.5% of the beam length are named respectively A_4 and A_3 (Fig.10b) in the first mode shape. It is observed that the ratio $\frac{A_3}{A_4} = 4.39$ is very close to the ratio $\frac{A_1}{A_2} = \frac{A_5}{A_6} = 4.34$, confirming the reliability of the proposed analysis.

Numerical results

The Rayleigh damping coefficients α and β associated to the specimen without lumped mass have been obtained by fitting experimental tests by means of Eq.(33)-(34), and then introduced

	Unimodal linear	Unimodal first order nonlinearities	Unimodal second order nonlinearities	Multimodal
NRMSD	2.51%	1.32%	0.98%	0.82%
ω_{10}	247.1460	247.1485	247.1499	247.1521
ω_{12}	0	0	145.9256	154.54075
ω_{14}	0	0	0	292.50608
ξ_{10}	0.0091	0.0089	0.0063	0.0077
ξ_{11}	0	0	0.01	0.7946
ξ_{12}	0	0	0	0
B_1	0.0049	0.0049	0.0046	0.0051
ϕ_1	1.3230	1.3228	1.3111	1.3090
ω_{20}	0	1549	1549.1	1549.4
ξ_{20}	0	0.004	0.0038	0.0041
B_2	0	-0.000884	-0.000884	-0.000826
ϕ_2	0	-0.1368	-0.1449	-0.1468

Table 3: FTH fitting coefficients for the signal at 39% of the beam length

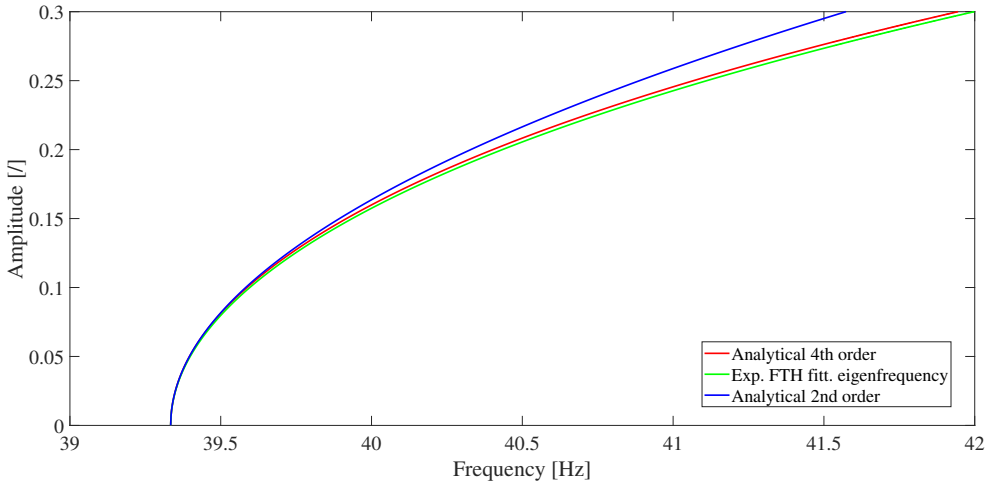

Fig. 9: Comparison of backbone curves determined by experimental and analytical methods

into the numerical simulations. They are:

$\alpha = 5.9744 \times 10^{-1}$,

$\beta = 3.7963 \times 10^{-5}$

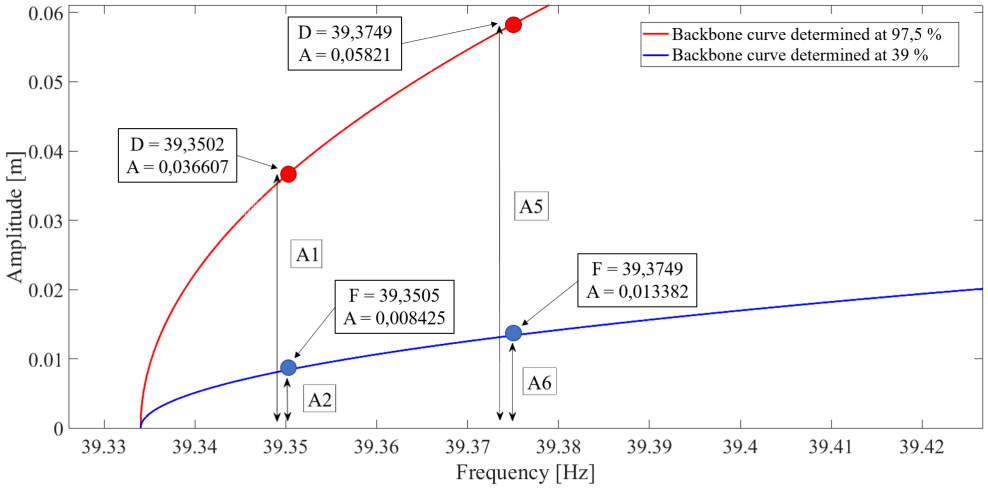

(a) Backbone curves obtained at 39% and 97.5% of the beam length.

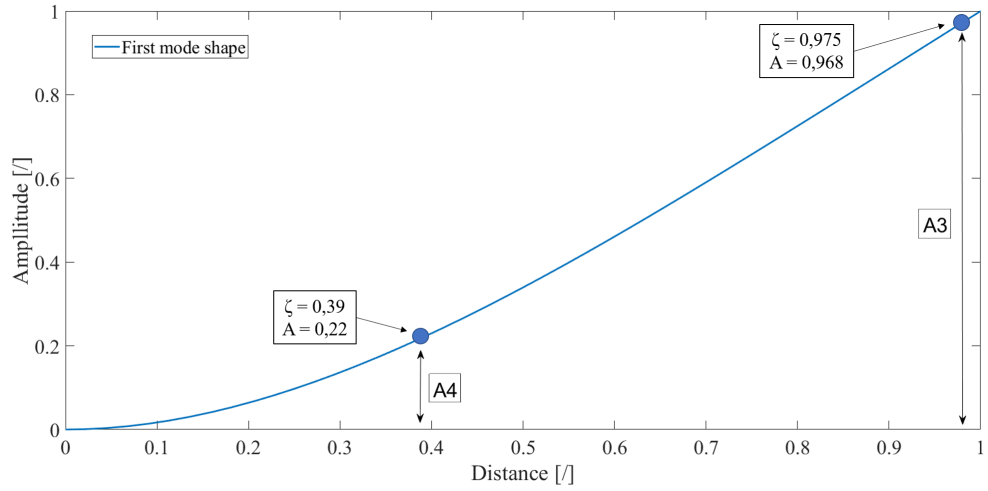

(b) First mode. Displacement amplitude along the beam.

Fig. 10: Comparison between the amplitude ratios

As aforementioned, the displacement time history obtained from the finite element simulation has been post-processed by the FTH method, obtaining for the first frequency the backbone curve shown in Fig.11. The results of the identification are reported in Tab. 4.

It can be noted that also the backbone curve obtained by numerical method is very similar to that obtained with the analytical formulation. In the same way of experimental investigation, multimodal identification increases the performance of the FTH. Indeed, inserting the second mode with its relative nonlinearities, the backbone curve of first frequency approaches that obtained analytically.

	Unimodal linear	Unimodal first order nonlinearities	Unimodal second order nonlinearities	Multimodal
NRMSD	1.19%	0.83%	0.42%	0.26%
ω_{10}	247.1485	247.1494	247.1538	247.1542
ω_{12}	0	103.2141	126.2579	154.2428
ω_{14}	0	0	245.5231	265.1426
ξ_{10}	0.0091	0.0091	0.0090	0.0090
B_1	0.24264	0.24265	0.24268	0.24269
ϕ_1	1.0249	1.0184	1.0170	1.0907
ω_{20}	0	0	0	1563.2
ξ_{20}	0	0	0	0.0041
B_2	0	0	0	0.00102
ϕ_2	0	0	0	2.4167

Table 4: FTH fitting coefficients for the numerical signal at 97.5 % of the beam lenght

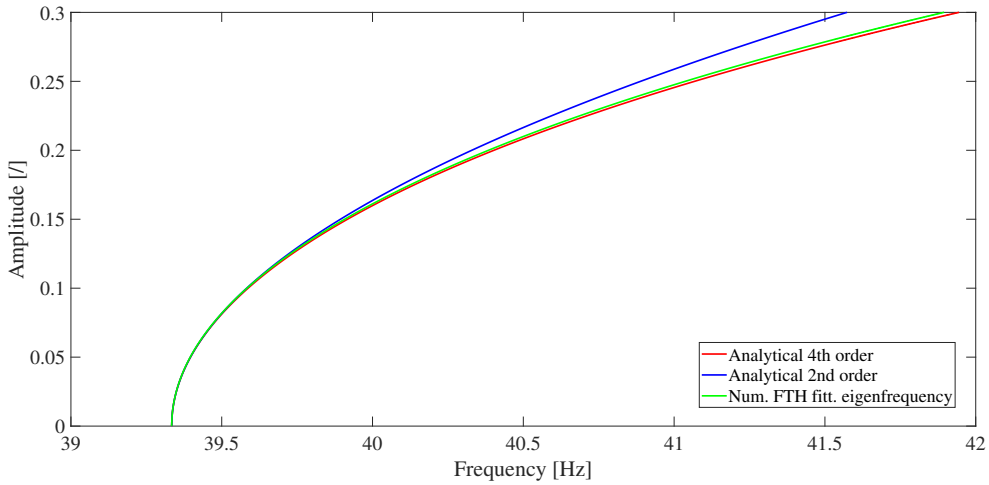

Fig. 11: Comparison of backbone curves determined by numerical and analytical methods

Overall comparison

This section shows the comparison of the backbone curves obtained by analytical, numerical (multimodal FTH) and experimental methods (multimodal FTH). Firstly, the backbone curve of the beam without lumped mass was considered. Secondly, the backbone curves with lumped masses were argued. This last backbone curves were not explicitly mentioned in the above sections

but they were obtained by adding the masses to the beam and doing the same procedure as in Experimental and Numerical Sections.

Fig.12 shows the comparison of backbone curves of cantilever beam without lumped mass; the results are in excellent agreement among each other. We can conclude that in this case the analytical and numerical model could foresee the experimental behavior.

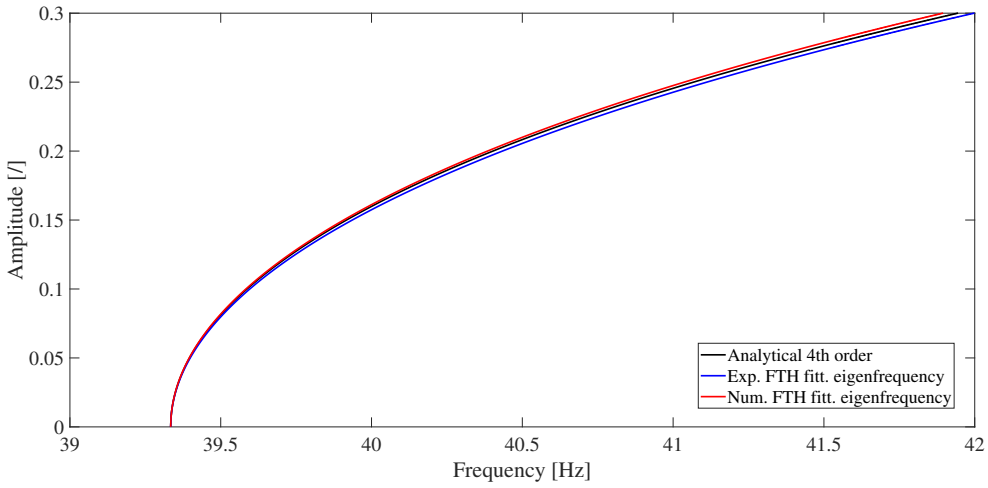

Fig. 12: Comparison of backbone curves of cantilever beam without lumped mass

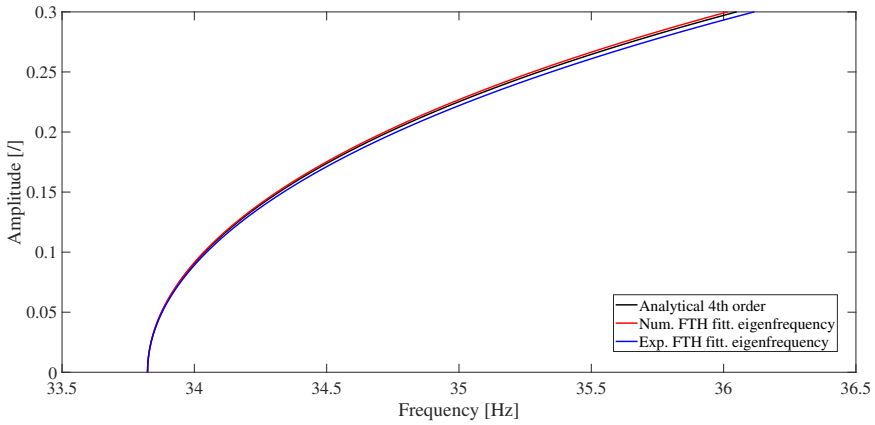

(a) 10% of the beam mass at 97.5% of the beam lenght

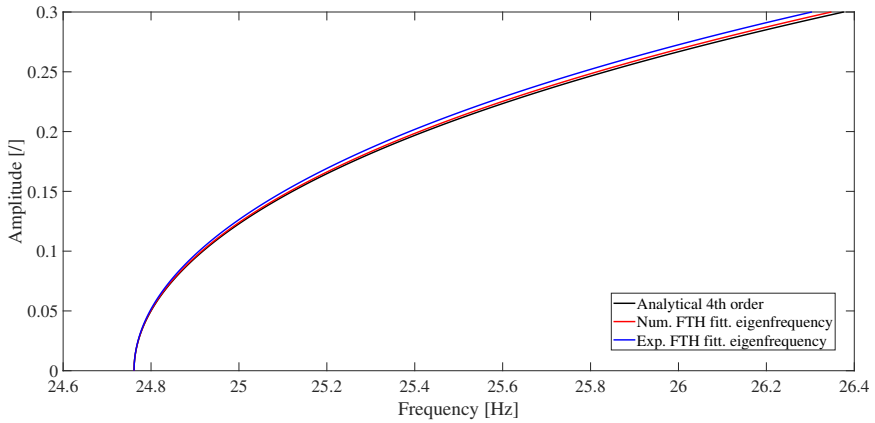

(b) 50% of the beam mass at 97.5% of the beam lenght

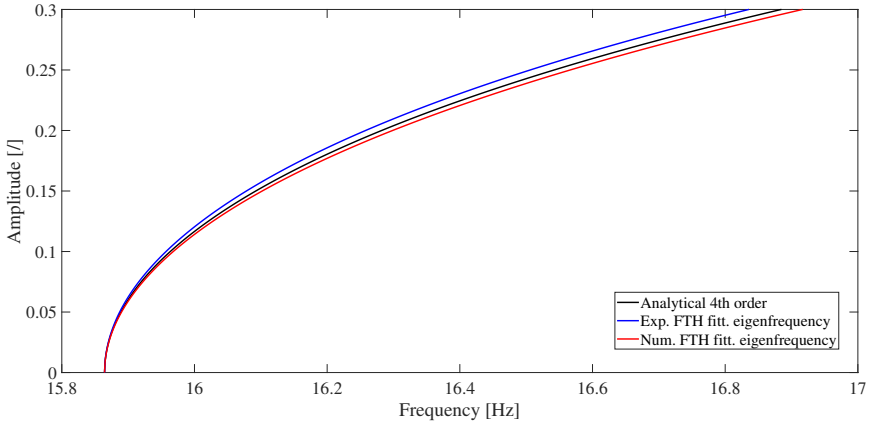

(c) 150% of the beam mass at 97.5% of the beam lenght

Fig. 13: Comparison of backbone curves of cantilever beam with lumped mass

Now a lumped mass is added on the beam at 97.5% of the beam length. Fig.13 shows the comparisons of backbone curves of cantilever beam with lumped mass of 10%, 50%, and 150% of the beam mass. All these cases show that the backbone curves are still consistent among each other, even if the mass is increased. The addition of mass determines only small differences between the three results. Thus, also in these cases the analytical and numerical model could foresee the experimental behavior.

When the concentrated mass is further increased the results start to diverge, as shown in Fig.14 for the cases of 300% of the beam mass. Consequently, the result shows the limit of analytical method to predict the nonlinear frequency. This confirms the lack of accuracy of the solution when the mass ratio μ exceeds the value of 3, as argued by Hamdan [15].

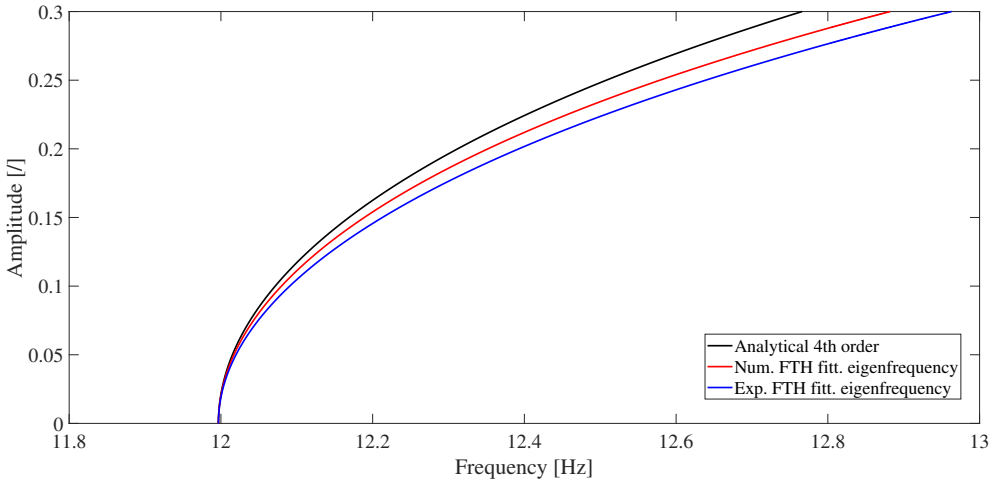

Fig. 14: Comparison of backbone curves of cantilever beam with a 300% of the beam mass at 97.5% of the beam length

CONCLUSION

This paper investigated the nonlinear dynamic behavior in large displacements of a cantilever beam without and with lumped mass fixed on its length. The analysis compared the results coming from analytical approach with numerical modelling and experimental observations. The results showed that the formulation describes the real backbone curve of the beam, which is hardening. The importance of inertial terms in the analytical modelling has been discussed.

The experimental and numerical data have been processed by Fitting Time History Method; the results confirmed the effectiveness of the FTH method to extract the modal terms from both experimental and numerical signals. The backbone curves obtained by the three methods are consistent with each other until the lumped mass is less than or equal to three time the mass of the beam mass. Above the results start to diverge.

Results show a harder experimental and numerical backbone curves than the analytical one. This behavior is explained by the fact that the eigenfunction used in the analytical expression of the backbone curve does not account for the lumped mass.

REFERENCES

[1] Hinnant H. E., and Hodges D. H., 1988. "Nonlinear analysis of a cantilever beam". *AIAA Journal,* **26**(12), pp. 1521–1537.

[2] Zavodney L. D., and Nayfeh A. H., 1989. "The non-linear response of a slender beam carrying a lumped mass to a principal parametric excitation: theory and experiment". *International Journal of Non-Linear Mechanics,* **24**(2), pp. 105–125.

[3] Crespo da Silva M. R. M., and Glynn C. C., 1978. "Nonlinear flexural-torsional dynamics of inextensional beams II. Forced motions". *Journal of Structural Mechanics,* **6**(4), pp. 449–461.

[4] Awrejcewwicz J., Kryosko A. V., and Soldatov V., 2012. "Analysis of the nonlinear dynamics of the timoshenko flexible beams using wavelets". *Journal of Computational and Nonlinear Dynamics,* **7**(1).

[5] Eisley J. G., 1964. "Nonlinear deformation of elastic beams, rings and strings". *Wear,* **7**(3), pp. 225–312.

[6] Beléndez T., Neipp C., and Beléndez A., 2002. "Large and small deflections of a cantilever beam". *European Journal of Physics,* **23**(3), p. 371.

[7] Navaee S., and Elling R. E., 1991. "Large deflections of cantilever beams". *Transactions of the Canadian Society for Mechanical Engineering,* **15**(1), pp. 91–107.

[8] Anderson T. J., Nayfeh A. H., and Balachandran B., 1996. "Experimental verification of the importance of the nonlinear curvature in the response of a cantilever beam". *Journal of*

Vibration and Acoustics, **118**(1), pp. 21–27.

[9] Babilio E., and Lenci S., 2017. "On the notion of curvature and its mechanical meaning in a geometrically exact plane beam theory". *International Journal of Mechanical Science,* **128-129**, pp. 277–293.

[10] Zheng Y., Shabana A. A., and Zhang D., 2018. "Curvature expressions for the large displacement analysis of planar beam motions". *Journal of Computational and Nonlinear Dynamics,* **13**(1).

[11] Lenci S., Clementi F., and Rega G., 2016. "A comprehensive analysis of hardening/softening behavior of shearable planar beams with whatever axial boundary constraint". *Meccanica,* **51**(11), pp. 2589–2606.

[12] Meesala V. C., and Hajj M. R., 2019. "Response variations of a cantilever beam–tip mass system with nonlinear and linearized boundary conditions". *Journal of Vibration and Control,* **25**(3), pp. 485–496.

[13] Sedighi H. M., and Shirazi K. H., 2012. "A new approach to analytical solution of cantilever beam vibration with nonlinear boundary condition". *Journal of Computational and Nonlinear Dynamics,* **7**(3).

[14] McHugh K. A., and Dowell E. H., 2019. "Nonlinear response of an inextensible, cantilevered beam subjected to a nonconservative follower force". *Journal of Computational and Nonlinear Dynamics,* **14**(3).

[15] Hamdan M. N.and Shabaneh N. H., 1997. "On the large amplitude free vibrations of a restrained uniform beam carrying an intermediate lumped mass". *Journal of Sound and Vibration,* **199**(5), pp. 711–736.

[16] Hamdan M. N., and Dado M. H. F., 1997. "Large amplitude free vibrations of a uniform cantilever beam carrying an intermediate lumped mass and rotary inertia". *Journal of Sound and Vibration,* **206**(2), pp. 151–168.

[17] Wagner H., 1964. "Large-amplitude free vibrations of a beam". *Journal of Applied Mechanics,* **32**(4), pp. 887–892.

[18] H. L. Wu, J. Yang, and S. Kitipornchai, 2016. "Nonlinear vibration of functionally graded

carbon nanotubereinforced composite beams with geometric imperfections". *Composite Part B,* **90**.

[19] L. L. Ke, J. Kang, and S. Kitipornchai, 2010. "Nonlinear free vibration of functionally graded carbon nanotube-reinforced composite beams". *Composite Structures,* **92**.

[20] C. Feng, J. Yang, and S. Kitipornchai, 2017. "Nonlinear free vibration of functionally graded polymer composite beams reinforced with graphene nanoplatelets (gpls)". *Engineering Structures,* **140**.

[21] Lenci S., Consolini L., and Clementi F., 2017. "The use of the Fitting Time Histories method to detect the nonlinear behaviour of laminated glass". *Journal of Vibration Testing and System Dynamics,* **1**(1), pp. 1–14.

[22] Lenci S., Consolini L., Clementi F., and Cocchi G., 2017. "Revealing nonlinear dynamical behaviour of laminated glass". *Procedia Engineering,* **199**, pp. 1454–1459.

[23] S. N. Mahmoodi, N. Jalili, and S. E. Khadem, 2008. "An experimental investigation of nonlinear vibration and frequency response analysis of cantilever viscoelastic beams". *Journal of Sound and Vibration,* **311**.

[24] Nayfeh A. H., 2000. *Perturbation methods*. John Wiley & Sons.

[25] Hijmissen J.W., and Van Horssen W.T, 2007. "On aspects of damping for a vertical beam with a tuned mass damper at the top". *Nonlinear Dynamics,* **50**(4).

[26] Hijmissen J.W., and Van Horssen W.T, 2008. "On the weakly damped vibrations of a vertical beam with a tip-mass". *Journal of Sound and Vibration,* **310**(3).

[27] Schwalbe D., and Wagon S., 1997. *The Duffing equation*. John Wiley & Sons.

[28] W. H. Liu, and C. C. Huang, 1988. "Free vibration of restrained beam carrying concentrated masses". *Journal of Sound and Vibration,* **123**(1).

[29] M. N. Hamdan, and L. A. Latif, 1994. "On the numerical convergence of dicretization methods for the free vibrations of beams with attached intertia elements". *Journal of Sound and Vibration,* **169**(4).

[30] M. Gindy, R. Vaccaro, and H. Nassifand J. Velde, 2008. "On the numerical convergence of dicretization methods for the free vibrations of beams with attached intertia elements".

Comput-Aided Civ. Inf., **23**.

[31] P. K. Kropp, 1997. “Experimental study of the dynamic response of highway bridges”. *Joint highway research Project No. C-36-56S, Purdue University, Indiana*.